PET Quantification in Neuropsychiatry

2

Michel Koole, Cindy Casteels, and Koen Van Laere

Contents

Abstract

PET quantification in neuropsychiatry focuses on the quantification of dynamic brain PET data. Starting from the basics of dynamic PET imaging, different methodologies are presented to extract time-dependent activity concentration for specific brain regions, both manually and automatically. The latter methodology uses predefined VOI templates and has the advantage of being operator independent. Once time-activity curves are available for the brain regions of interest,

M. Koole (✉)
Department of Nuclear Medicine and Molecular Imaging,
University Medical Center Groningen, University of Groningen,
Hanzeplein 1, Groningen 9700 RB, The Netherlands
e-mail: m.koole@umcg.nl

C. Casteels • K. Van Laere
Division of Nuclear Medicine, Department of Imaging and Pathology,
University Hospitals Leuven, KU Leuven, Leuven, Belgium

Nucleaire Geneeskunde en Moleculaire Beeldvorming,
Katholieke Universiteit Leuven, Universitair Ziekenhuis,
Herestraat 49, Leuven 3000, Belgium

R.A.J.O. Dierckx et al. (eds.), *PET and SPECT in Psychiatry*,
DOI 10.1007/978-3-642-40384-2_2, © Springer-Verlag Berlin Heidelberg 2014

kinetic modeling is described using different compartmental models. These compartments represent the different states of the radiotracer such as the bound state. This way, the PET signal of specifically tracer can be separated from tracer that is free or nonspecifically bound. In this context, quantitative endpoints such as distribution volume and binding potential are discussed. Next to compartment modeling, graphical analysis techniques for reversible and irreversible tracer kinetics are discussed. These techniques are computational efficient and therefore suitable for creating parametric image data. These parametric image data allow voxel-wise statistical comparison of dynamic PET data. In terms of different options for the input function which is needed for tracer kinetic modeling, we discuss different possibilities including a reference tissue model. Finally, we elaborate on the advantages and limitations of a bolus/constant infusion approach to quantify tracer uptake under steady-state conditions.

2.1 Introduction

Functional neuroimaging has been an established research tool in neuropsychiatry demonstrating relationships between behavioral and neurobiological factors. Among functional imaging modalities, magnetic resonance spectroscopy (MRS) allows mapping of the distribution and concentration of metabolites involved in neuro-energetics and amino acid neurotransmission (Puts and Edden 2012). Especially glutamate/glutamine and γ-aminobutyric acid (GABA)/glutamine cycles appear to be sensitive to psychiatric disorders such as depression (Duman and Aghajanian 2012; Kendell et al. 2005; Sanacora et al. 2012; Walter et al. 2009). On the other hand, functional magnetic resonance imaging (fMRI) measures the neural activity indirectly and is able to study alternations in the steady-state functional connectivity related to major depressive disorder (Enzi et al. 2012; Greicius 2008; Kühn and Gallinat 2013).

Positron Emission Tomography (PET) and in particular brain PET enables the in vivo mapping of neurobiological functions such as blood flow (Kim et al. 2009), metabolism (Luyten et al. 2012), enzyme activity, neuro-receptor binding site density (Gérard et al. 2011), or occupancy (Van Laere et al. 2012). A typical PET study involves the injection of a radiotracer (a compound labeled with a radionuclide) into the venous blood stream of a subject. This radiotracer is delivered to the brain by the arterial flow, and after crossing the blood–brain barrier, it might bind reversibly or irreversibly to neuro-receptors and transporter vesicles or be metabolized by endogenous enzymes. On the other hand, if the tracer is inert, it would diffuse across the blood–brain barrier and would not be bound or trapped. In parallel to these biochemical processes, the radioisotope label will decay, emitting a positron that annihilates to emit diametrically opposed 511 keV photons. Part of these photon pairs will be detected by PET scanner within a predefined timing window (usually 6–10 ns) as a pair of coincidence detections. Therefore, PET is also being referred to as coincidence imaging. Over the total duration of the scan (usually 1–2 h), emission data are acquired, corrected for physical effects such as attenuation and scatter

and binned into different time frames. The corrected data of each time frame are reconstructed using an analytical or iterative reconstruction algorithm to generate a three-dimensional image of the radiotracer distribution in the brain over various time intervals.

PET imaging has been used extensively to explore a variety of biochemical, physiological, and pharmacological processes and to study aspects of the complex interaction of several neurotransmitter systems in the brain (Kenneth et al. 2002; Savitz and Drevets 2013; Smith and Jakobsen 2009). Compared to MR-based techniques, PET has the particular advantage that it is highly sensitive and quantitative. Moreover, PET can quantify nano-molar molecular concentrations without any pharmacological effects. The amount of tracer injected is a trace amount and causes no changes in the physiology of the organism. In terms of PET tracer development, labeling the appropriate precursor is not the major obstacle since most candidate ligands contain carbon and hydrogen such that a positron emitting nuclide can be incorporated as an isotopic variant or atomic substitute. The most challenging to the development of in vivo PET tracers is actually the relatively small window of an appropriate combination of lipophilicity, molecular weight, and affinity.

Several radiolabeled molecules have been developed targeting specific receptor systems of interest in psychiatric disorders. Next to the serotonin and dopaminergic brain function, PET imaging of neuroinflammation and the endocannabinoid system has been proven very interesting especially in relation to schizophrenia (Doorduin et al. 2009; Wong et al. 2010) and alcohol dependence (Hirvonen et al. 2012). Besides synaptic targets, post-receptor signal transduction has gained interest since abnormalities in second messenger systems could play an important pathophysiological role in many psychiatric diseases. One of the major biochemical cascades in this context is the cyclic adenosine monophosphate (cAMP) signal transduction system. Recently, an antagonist PET tracer has been developed for the dual-substrate enzyme phosphodiesterase 10A (PDE10A) (Van Laere et al. 2013) (see Fig. 2.1) which is part of this cascade system and has a restricted distribution, predominantly in the human brain and more specifically in medium spiny neurons (MSNs) of the striatum, substantia nigra, nucleus accumbens, and the olfactory tuberculum (Seeger et al. 2003; Tu et al. 2011). This enzyme mainly hydrolyzes the important second messengers cyclic adenosine monophosphate (cAMP) (Bender and Beavo 2006; Fujishige et al. 1999), downregulating protein kinase A (PKA) activity (Nishi et al. 2008), and therefore the phosphorylation of various intracellular targets downstream of PKA such as DARPP-32 as an integrator of dopamine and glutamate signals (Surmeier et al. 2007). This role in striatal signaling has made PDE10A an enzyme of particular interest as it is likely involved in several neuropsychiatric and neurodegenerative disorders (Hebb and Robertson 2007; Siuciak and Strick 2006). For instance, PDE10A protein levels of Huntington's disease (HD) patients are reduced in the caudate nucleus and putamen compared with samples from age-matched controls (Hebb et al. 2004), while the progressive loss of PDE10A in two different HD transgenic mice strains correlates with progression and severity of motor symptoms. PDE10A inhibition may constitute a new approach for the treatment of HD and of other disorders with

altered MSN activity, such as schizophrenia (Grauer et al. 2009) and addiction (Menniti et al. 2006). In this context, a suitable PDE10A tracer that allows in vivo quantification of PDE10A would lead to a better understanding of the role of PDE10A activity in specific disease states. Moreover, this tracer could be used as a tool for early clinical evaluation of emerging PDE10A medication and may also present new diagnostic opportunities.

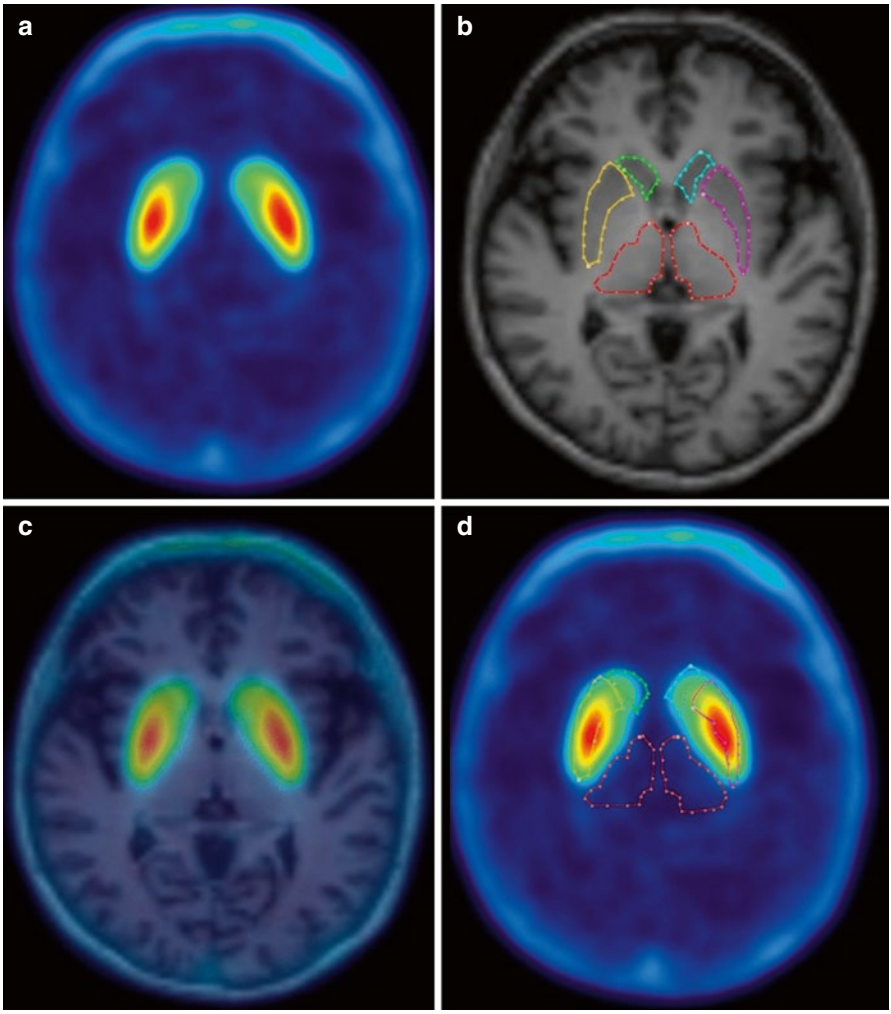

Fig. 2.1 Time-activity curves of a PET tracer targeting PDE10A (Van Laere et al. 2013) for the putamen, caudate nucleus, and thalamus. (**a**) represents an average SUV image (averaged over 60–90 min interval), (**b**) the corresponding T1-weighted MRI dataset with delineated brain structures, (**c**) the co-registered MR and PET dataset, and (**d**) the PET dataset with the brain structures transferred from the registered MR dataset

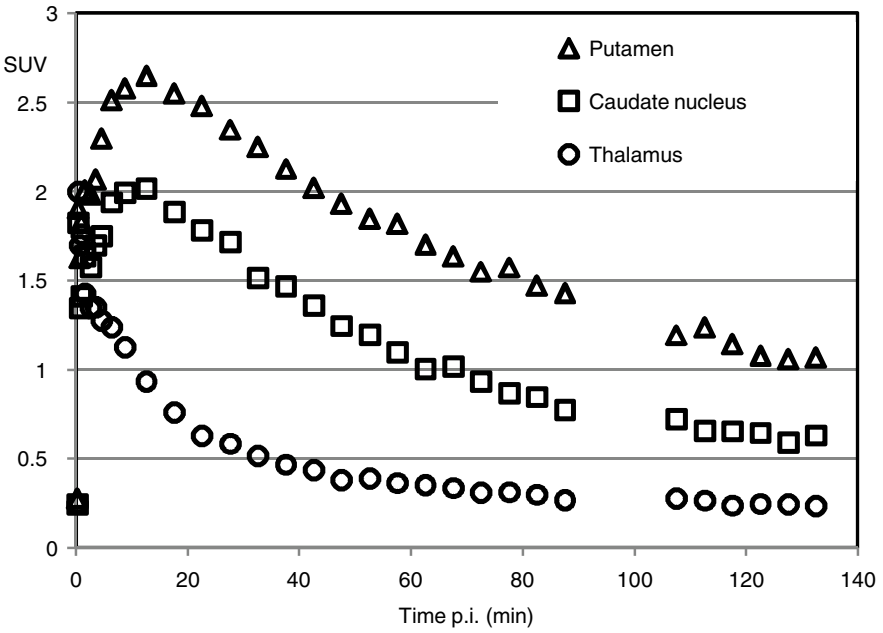

Fig. 2.1 (continued)

Since each PET probe is characterized by its particular kinetic behavior in the brain, understanding its dynamics and quantification is a critical component for designing imaging protocols, setting up clinical studies and interpreting results.

2.2 Dynamic PET Quantification

In vivo quantification of molecular targets with PET imaging is complicated due to the fact that tracers are administered intravenously and not directly applied to the target tissue. Therefore, delivery of the tracer to the brain is influenced by the local blood flow, free tracer concentration in the plasma, and peripheral tracer clearance due to metabolization and excretion. Moreover, total brain activity is measured with PET brain imaging, while often specifically bound, nonspecifically bound, and free tracer need to be separated to estimate the specific tracer signal. For the remainder, we assume that appropriate algorithms have been used to reconstruct a quantitative, accurate radiotracer distribution such that image values are proportional to the radiotracer concentration in brain tissue. We will focus on the accurate quantification of the particular neurobiological function targeted by the radiotracer. Therefore, three essential aspects are to be considered. On the one hand, dynamic PET data characterize the kinetic behavior of the PET tracer in brain tissue, while, on the

other hand, an input function is needed to describe the time-dependent amount of tracer that is delivered to the brain tissue. Third, relatively complicated mathematical analysis will model the tracer kinetics on basis of the dynamic PET data and an input function.

Dynamic PET image data are binned and reconstructed into various time frames and represent the radiotracer distribution in tissue at specific time points throughout the PET study. This temporal evolution of radiotracer concentration in individual voxels or regions of the image volume is called a time-activity curve (TAC). These TACs form the basis in quantifying the physiological (e.g., blood flow) and/or pharmacological aspect (e.g., receptor binding site density, enzyme activity) of the system of interest.

To generate TAC for specific brain regions of interest, PET data can be aligned with corresponding MRI data by optimizing translation and rotation parameters. This way high-resolution anatomical MR information can be used to facilitate manual delineation of the appropriate volume-of-interest (VOI) especially when the PET data itself provide limited anatomical landmarks (see Fig. 2.1).

While manual delineation can be time-consuming and observer dependent, methodologies have been developed that allow automatic VOI generation (Svarer et al. 2005). These methods create an individualized VOI probability map on the basis of a database of several MRI datasets, where a VOI template has been defined manually on each MRI dataset. Nonlinear image registration between these MRI datasets and the MRI dataset of interest allows transfer of these individually defined VOI templates to the MRI dataset of interest. Based on the degree of overlap of the transferred VOI sets, a VOI probability map is created specifically for that particular PET dataset. When the generated VOI map is based on more than one template VOI set, VOI delineation proved to be better reproducible and showed less variation as compared to manual delineation or transfer of only a single VOI template. This methodology allows a fast, objective, and reproducible assessment of regional brain PET values.

In addition, the latter methodology offers the possibility to correct for partial volume effects in brain PET imaging. Due to the limited resolution of PET imaging, a PET voxel is only partly composed of the target brain tissue which in most cases is a specific grey matter brain structure. Therefore, the PET signal actually reflects the activity concentration of different underlying adjacent tissue types like the grey matter, white matter, and cerebrospinal fluid. Because of differences in activity concentration between these tissue compartments, the PET signal of the target tissue is confounded. One can correct for this partial volume effect by using spatial distribution maps for the white matter, grey matter, and cerebrospinal fluid generated from segmented co-registered MRI data. Taking into account the resolution of the PET system, it is possible to estimate the different underlying tissue fractions for each PET voxel and apply an appropriate correction and weighting of the PET signal (Rousset et al. 2007). This way, the actual tracer uptake per unit grey matter tissue can be determined. This especially applies when comparing healthy volunteers with elderly subjects or with patients suffering from psychiatric disorders where the presence of regional cerebral atrophy is suspected.

In terms of mathematical analysis, brain uptake of a radioactive tracer is often described within the theoretical framework of compartments. Compartment modeling allows description of systems that vary in time but not in space as one of the assumptions for compartmental modeling is that there are no spatial concentration gradients within each department but only gradients in time. In fact, a compartment represents a unique state of the tracer and is defined as a space with separate uptake and clearance rate constants where the radioactive tracer concentration is assumed homogeneous. Rate constants of each compartment are assumed time invariant at least over the duration of the study and considered being representative for the steady state of the system and the properties of the ligand. A compartment may have a physical analog such as interstitial fluid compartment but can also be considered as a tracer being in bound or unbound state. Once the exchange paths between compartments have been specified, the mass balance for each compartment can be described as a set of ordinary differential equations where one differential equation corresponds to an unknown tracer concentration. Tracer concentration in the vascular arterial compartment drives the model taking into account that tracer tissue concentrations are zero at the start of the PET study.

The first compartmental model that was described is the diffusion model for regional cerebral perfusion PET imaging (Frackowiak et al. 1980).

2.3 Compartmental Modeling of Brain Perfusion

PET can be used to study neuronal activation by measuring the changes in regional cerebral perfusion and local large vessel blood flow since changes in neuronal activity are very closely related to perfusion. These PET studies use blood flow tracers like water or butanol which enter brain tissue via diffusion Perhaps it is worthwhile noticing that the term perfusion is used to distinguish the blood flow per unit tissue from the physical flow (ml/min), although the term flow and perfusion has been used interchangeably in the literature.

Kety and Schmidt first described this basic exchange model for nonradioactive substances using the Fick principle (Kety and Schmidt 1948). The Fick principle states that when a fluid with known flow F runs through a compartment which is in steady state, the rate at which substance is extracted from the fluid by the compartment is equal to the difference in concentration when entering and leaving the compartment. Applying this principle to the passage of tracer within capillaries and considering the smallest scale such that the blood compartment represents a single capillary and the compartment is the tissue in the immediate vicinity (see Fig. 2.2), the change in tracer concentration in tissue C_T can be described as difference in tracer concentration between arterial blood C_A and venous blood C_V:

$$\frac{dC_T(t)}{dt} = F\left(C_A(t) - C_V(t)\right). \tag{2.1}$$

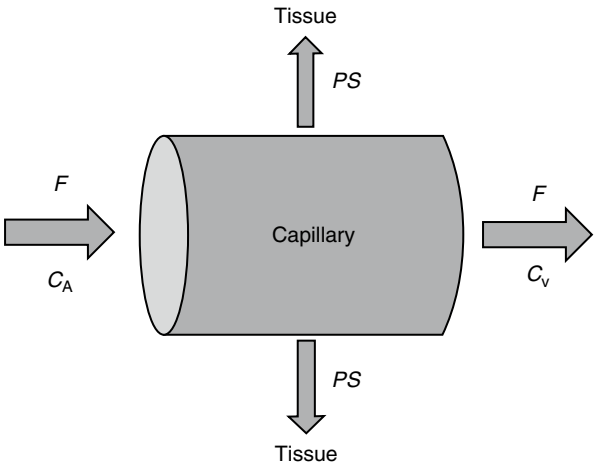

Fig. 2.2 Schematic overview of the exchange of a substance between capillary and tissue where C_A denotes the concentration of a substance in arterial blood, C_V the concentration in the venous blood, F the flow (units per min), and PS the product of the permeability P (cm/min) and the surface S (cm^2/g) of the capillary

In this context, the partition coefficient ρ was defined as the ratio of the tissue to venous blood concentration. For tracers with high extraction, one can assume that tracer concentration in the venous blood will be in equilibrium with the tissue concentration. Therefore, the tracer concentration in tissue C_T is described by

$$\frac{dC_T(t)}{dt} = FC_A(t) - \frac{F}{\rho}C_T(t). \tag{2.2}$$

Since tracer concentration can be measured in arterial blood and in tissue and one typically assumes that the same input function is valid for all brain tissue, Eqn. (2.2) can be solved for blood flow and partition coefficient as a function of tissue and arterial blood concentration. Note that this model is only valid when blood flow remains constant during PET imaging and the PET tracer is inert and rapidly and freely diffusible in brain tissue.

2.4 One-Tissue Compartmental Model

The partition coefficient in the context of high extraction tracers can be defined more generally as the ratio of the steady-state concentrations between two compartments and is numerically identical to the tissue volume of distribution V_T. The distribution volume is often used in PET literature and is defined as the apparent volume a tracer would occupy, if the tracer were to adopt the same concentration in tissue as in blood. In steady-state PET studies where tracer is delivered via constant infusion in order to maintain tracer concentration in the arterial blood at a constant level, the distribution volume is easily derived from constant concentration ratios in equilibrium. In dynamic PET studies, however, we measure time-dependent concentrations. Assuming that the system is in steady state and the so-called tracer

assumption is valid that tracer concentration is negligible, the degree of substance exchange (such as transport through one or more membranes, enzymatic conversions, or binding to specific sites) between kinetically defined "compartments" is proportional to the concentration and can be quantified by rate constants, and rate constants between kinetic compartments are estimated. From these rate constants, the distribution volume can be derived as well. However, if we want to estimate the rate constants, we need to take into account that PET measures all activity present in the field of view, both intra- and extravascular. Thus, the total activity concentration measured by the PET system $C_{PET}(t)$ is given by

$$C_{PET}(t) = (1 - V_B) C_T(t) + V_B C_B(t). \tag{2.3}$$

V_B represents the blood fraction present in the field of view ($0 \leq V_B \leq 1$) and $C_B(t)$ the activity concentration in the whole blood, while $C_T(t)$ stands for the activity concentration in brain tissue. For the human brain, the assumption that blood occupies about 5 % of the brain volume is valid (Phelps et al. 1979), corresponding to a V_B value of about 0.05.

Considering a one-tissue compartment model for describing the bidirectional flux of tracer between blood and tissue, this model is characterized by the time-varying tracer concentration in tissue $C_T(t)$ and the arterial blood $C_A(t)$ and two first-order kinetic rate constants K_1 and k_2. This way the tracer flux from blood to tissue is $K_1 C_A$, while the tracer flux from tissue to blood is $k_2 C_T$. Therefore, the net tracer flux into tissue is describes as

$$\frac{dC_T(t)}{dt} = K_1 C_A(t) - k_2 C_T(t). \tag{2.4}$$

$C_T(t)$ represents the radioactivity concentration that is measured with PET in a given brain region, while blood samples may be drawn during the PET measurement in order to measure $C_A(t)$.

If we consider tracer exchange on its smallest scale between a blood capillary and the surrounding tissue (see Fig. 2.2), the fraction that is extracted during one capillary pass is equal to

$$E = \frac{C_A - C_V}{C_A}. \tag{2.5}$$

If we take into account the boundary condition that during the first pass of tracer through tissue the tracer flux from tissue to blood is effectively zero because $C_T(0) = 0$ and apply this boundary condition to (2.1) and (2.4), the following equation is valid:

$$\frac{dC_T(t)}{dt} = K_1 C_A(t) = (FE) C_A(t). \tag{2.6}$$

This indicates that the delivery rate constant K_1 equals the product of blood flow and first pass extraction fraction. Considering the capillary as a cylindrical tube, the extraction fraction can be interpreted using the Renkin-Crone capillary model (Crone 1963; Renkin 1959) which states that

$$E = \frac{C_A - C_V}{C_A} = 1 - \exp\left(-\frac{PS}{F}\right). \tag{2.7}$$

In this equation, P is the permeability of the capillary membrane and S is the capillary surface area per unit tissue mass. Using this approximation the following equation for K_1 is valid:

$$K_1 = F\left(1 - \exp\left(-\frac{PS}{F}\right)\right). \tag{2.8}$$

This means that K_1 is closely related to blood flow when the extraction fraction is large ($PS >> F$) but is more related to permeability when the extraction fraction is low. Accordingly, the best tracers for studying blood flow have a large extraction fraction. For a freely diffusible tracer, K_1 equals perfusion and the ratio $\frac{K_1}{k_2}$ equals the partition coefficient ρ. In a more general context, if we consider tracer concentrations in blood and tissue in equilibrium, a state with no net transfer of tracer between the two compartments, the gradient $\frac{dC_T(t)}{dt}$ in (2.4) can be set to zero and the following equation for the distribution volume V_T is valid:

$$V_T = \frac{C_T(t)}{C_A(t)} = \frac{K_1}{k_2}. \tag{2.9}$$

2.5 Two- and Three-Tissue Compartment Model

Partition coefficient ρ or distribution volume V_T can be considered as a potential quantitative endpoint of PET tracer uptake in the brain. However, for ligand-receptor PET studies, the law of mass action is applicable to ligand-receptor interaction, and under equilibrium conditions, the following equation is valid:

$$\frac{B}{F} = \frac{B_{max}}{K_d + F}. \tag{2.10}$$

In this equation, B represents the tracer concentration bound to the receptor, and F denotes the free tracer concentration near the receptor, while B_{max} refers to the receptor density and $1/K_d$ to the ligand affinity for the receptor (K_d is ratio of the dissociation constant k_{off} over the association constant k_{on}). Since PET imaging

typically involves the injection of a very limited amount of ligand mass dose, the concentration of free radiotracer is such that $F << K_d$, resulting in the following equation:

$$\frac{B}{F} = \frac{B_{max}}{K_d}. \tag{2.11}$$

This equation actually corresponds to the binding potential (BP) defined as the product of receptor density and affinity. In terms of PET imaging, this means that BP can be estimated as the equilibrium ratio of specifically bound tracer to free tracer and can be considered as a quantitative endpoint for ligand-receptor studies.

For radioligands that pass the blood–brain barrier by passive diffusion, one can reasonably assume that under equilibrium conditions, the concentration free tracer in arterial plasma equals the concentration free tracer in brain tissue. However, to estimate the concentration of specifically bound tracer, a one-tissue compartment model needs to be extended to a kinetic model containing multiple compartments. The most generalized kinetic model describing ligand-receptor kinetics consists of 3-tissue compartments (see Fig. 2.3), taking into account the activity concentration in arterial plasma C_P, the concentration of free radioligand in tissue C_F, the concentration of tracer that bounds specifically C_S, and the concentration of tracer that does not bound specifically C_{NS}, and therefore is not available for specific binding to the targeted receptor. In this context, K_1 and k_2 represent the transport rate constants between arterial plasma and tissue through the blood–brain barrier, and k_3 and k_4 describe the rate of specific binding and target release of the tracer, while k_5 and k_6 represents the exchange rate constants between the free tracer compartment and nonspecifically bound compartment. For a three-tissue compartment model, the activity concentration in brain tissue $C_T(t)$ is given by

$$C_T(t) = C_F(t) + C_{NS}(t) + C_S(t). \tag{2.12}$$

If we formulate the differential equations for the unknown tissue concentrations $C_F(t)$, $C_{NS}(t)$, and $C_S(t)$, we get the following equations:

$$\frac{dC_F(t)}{dt} = K_1 C_P(t) - k_2 C_F(t) - k_3 C_F(t) + k_4 C_S(t) - k_5 C_F(t) + k_6 C_{NS}(t), \tag{2.13}$$

$$\frac{dC_S(t)}{dt} = k_3 C_F(t) - k_4 C_S(t), \tag{2.14}$$

$$\frac{dC_{NS}(t)}{dt} = k_5 C_F(t) - k_6 C_{NS}(t). \tag{2.15}$$

Considering the equilibrium condition where no net exchange between compartments is observed, gradients in (2.13), (2.14) and (2.15) can be set to zero. Substitution

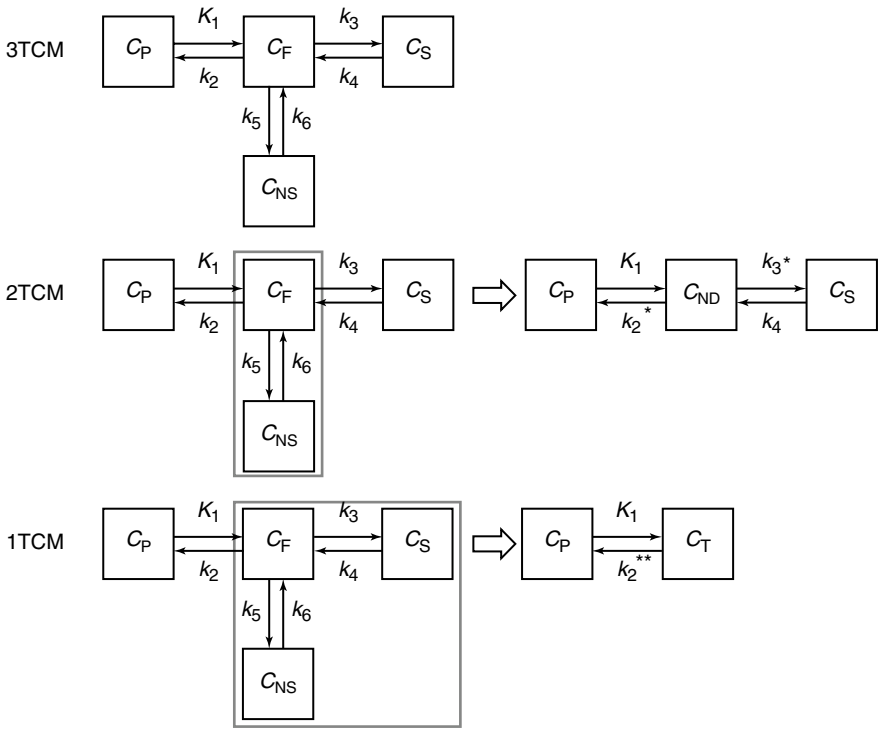

Fig. 2.3 Overview of the different compartment models: a three-tissue compartment model (3TCM) with C_P the activity concentration in arterial plasma, C_F the concentration of free radioligand in tissue, C_S the concentration of tracer that is bound specifically and C_{NS} the concentration of tracer that is bound nonspecifically, K_1 and k_2 represent the transport rate constants between arterial plasma and brain tissue, k_3 and k_4 represent the exchange rate constants between specific binding and the unbound state, while k_5 and k_6 represents the exchange rate constants between the free tracer and nonspecific binding. A two-tissue compartment model (2TCM) with C_P the activity concentration in arterial plasma, C_{ND} the concentration of non-displaceable radioligand in tissue, C_S the concentration of tracer that is bound specifically, K_1 and k_2^* represent the transport rate constants between arterial plasma and brain tissue, and k_3^* and k_4 represent the exchange rate constants between specific binding and the free and nonspecifically bound state. A one-tissue compartment model (1TCM) with C_P the activity concentration in arterial plasma, C_T the tracer concentration in tissue, and K_1 and k_2^{**} represent the transport rate constants between arterial plasma and brain tissue

of (2.14) and (2.15) in (2.13) yields the following equations for the distribution volume of free tracer, specific bound tracer, and nonspecific bound tracer:

$$V_F = \frac{C_F(t)}{C_P(t)} = \frac{K_1}{k_2}, \tag{2.16}$$

$$V_S = \frac{C_S(t)}{C_P(t)} = \frac{k_3}{k_4} V_F, \tag{2.17}$$

$$V_{NS} = \frac{C_{NS}(t)}{C_P(t)} = \frac{k_5}{k_6} V_F. \tag{2.18}$$

The total volume of distribution for brain tissue V_D can be written as

$$V_T = V_F + V_{NS} + V_S = \frac{K_1}{k_2}\left(1 + \frac{k_3}{k_4} + \frac{k_5}{k_6}\right). \tag{2.19}$$

If we consider equilibrium conditions for (2.14) and compare with (2.11), the following equation is valid:

$$\frac{k_3}{k_4} = \frac{V_S}{V_F} = \frac{C_S}{C_F} = \frac{B}{F} = \frac{k_{on} B_{max}}{k_{off}} = \text{BP}. \tag{2.20}$$

This means that BP can be estimated once the rate constants k_3 and k_4 are determined. Moreover, the rate constant k_3 is dependent on the density of available receptor sites and the ligand-receptor association constant k_{on}, while k_4 equals the ligand-receptor dissociation constant k_{off}.

When the transport rate constants k_5 and k_6 are high such that there is a fast equilibrium between the free tracer and nonspecifically bound tracer compartment, the two compartments are kinetically indistinguishable and can be lumped together into one compartment representing the non-displaceable tracer concentration $C_{ND}(t) = C_F(t) + C_{NS}(t)$. This model reduction yields a two-tissue compartment model with the following differential equations describing this model:

$$C_T(t) = C_{ND}(t) + C_S(t), \tag{2.21}$$

$$\frac{dC_{ND}(t)}{dt} = K_1 C_P(t) - k_2^* C_{ND}(t) - k_3^* C_{ND}(t) + k_4 C_S(t), \tag{2.22}$$

$$\frac{dC_S(t)}{dt} = k_3^* C_{ND}(t) - k_4 C_S(t). \tag{2.23}$$

The corresponding tissue distribution volume is given by

$$V_T = V_{ND} + V_S = \frac{K_1}{k_2^*}\left(1 + \frac{k_3^*}{k_4}\right). \tag{2.24}$$

In this case the quantitative parameter of interest is the non-displaceable binding potential BP_{ND} defined as

$$\text{BP}_{ND} = \frac{C_S}{C_{ND}} = \frac{V_S}{V_{ND}} = \frac{k_3^*}{k_4}. \tag{2.25}$$

It is worthwhile noticing that the non-displaceable binding potential BP_{ND} is defined relative to the concentration non-displaceable radiotracer, whereas the binding potential BP is defined relative to the concentration free radioligand (Innis and Carson 2007). In cases where nonspecific tracer binding could be excluded, BP and BP_{ND} are identical. Model reduction to a two-tissue compartment model is usually necessary for the kinetic analysis of dynamic PET data. This way, the number of unknown variables is reduced and more reliable estimates of the exchange rate constants can be achieved.

When the rate constants k_3^* and k_4 of a two-tissue compartment are high compared to transport rate constants K_1 and k_2^*, a fast equilibrium is achieved between the non-displaceable and specifically bound tracer compartment. In this case a further reduction to a single-tissue compartment is possible where kinetics described by (2.4) and (2.9) are valid.

If a specific brain region is devoid of receptors, the brain tissue of that region can be considered reference tissue. Consequently, BP_{ND} can be estimated for any target region using the tissue distribution volumes of reference and target tissue as follows:

$$BP_{ND} = \frac{C_S}{C_{ND}} = \frac{C_T - C_R}{C_R} = \frac{V_T - V_R}{V_R}. \tag{2.26}$$

C_T and V_T, respectively, represent the tracer concentration and distribution volume of the target region, while C_R and V_R, respectively, represent those of the reference region. It is worthwhile noticing that in this context $\frac{V_T(t)}{V_R(t)}$ is often termed the distribution volume ratio (DVR) such that $BP_{ND} = DVR - 1$.

We need to point out that in the absence of a reference region, BP or BP_{ND} can be estimated numerically but this estimate is often not reliable. The quantitative parameter that is used most frequently in the absence of reference tissue is the distribution volume V_T which can be estimated more reliably.

Equation (2.26) is valid if the tracer concentration in the reference region represents the non-displaceable tracer concentration and if the non-displaceable tracer concentration is the same for both reference and target region. If there is nonspecific tracer binding in the reference tissue and this nonspecific binding can again be assumed the same for both reference and target tissue, the binding potential BP_{ND} calculated from tissue distribution volumes will be biased. Taking into account the distribution volumes of both tissues, one gets the following equation:

$$BP_{ND} = \frac{V_T - V_R}{V_R} = \frac{V_S}{V_F + V_{NS}} = \frac{BP}{\left(1 + \frac{V_{NS}}{V_F}\right)}. \tag{2.27}$$

Assuming that the level of nonspecific binding is relatively constant, the bias should be limited to only a scaling factor.

2.6 Model Selection

The choice of a specific model configuration is governed by various factors including the properties of the tracer. To facilitate quantification radiotracers need to have appropriate chemical characteristics. For tracers that cross the blood–brain barrier via passive diffusion, a low molecular weight is mandatory. Lipophilicity of the tracer should be within the small range of allowing adequate permeability of the blood–brain barrier while avoiding unacceptable binding to plasma proteins or high levels of nonspecific binding in the brain. Finally, a high affinity ligand is needed to provide high levels of specific binding to the receptor. However, affinity of the tracer should be such that the opposing goals of high specific binding and washout of the brain are balanced.

If the tracer is inert and does not interact with any receptor system or does not undergo any chemical change, but simply diffuses into and back out of the cells, a one-tissue compartment model would be an appropriate model.

If a one-tissue model is not appropriate, the reversibility of a tracer or in other words the retention of the tracer in the target tissue must be considered prior to choosing the model configuration. Reliable estimates of receptor levels in the brain require both uptake and washout phases of the tissue time-activity curve. Therefore, the tissue clearance of the tracer must typically be matched with the half-life of the radionuclide. This tissue clearance rate is in part determined by the affinity of the tracer and the receptor density. Ligands with higher affinity targeting a rather dense population of receptors tend to stick longer to the target molecules such that washout is delayed beyond the usable measurement time of the radionuclide. If the affinity is such that the radioligand shows very modest washout from the brain during the course of the PET measurement, then the washout rate cannot be determined reliably and critical kinetic data are unavailable to calculate tissue distribution volume V_T, BP, or BP_{ND}. In terms of transport rate constants, this means that a reliable estimation of the k_4 parameter describing the conversion from the tracer trapped in the bound state back to the nonspecific state is not feasible. In this case and in cases where the tracer is metabolized and the metabolized state is retained in the brain tissue, the tracer can be considered to bind irreversible and k_4 of (2.23) can be set to zero. Instead of V_T, BP, or BP_{ND}, the influx rate constant K_i, also named metabolic rate, trapping rate, or accumulation rate constant, can be considered as an endpoint. K_i is defined as

$$K_i = K_1 \frac{k_3^*}{k_2^* + k_3^*}. \tag{2.28}$$

This assumption is, for instance, valid for measuring energy metabolism with 2-fluoro-2-deoxy-D-glucose labeled with the fluorine radioisotope ^{18}F ([^{18}F]-FDG). The substance is glucose analog that is trapped in brain tissue by being metabolized in the mitochondria to FDG-6-PO4 by the hexokinase enzymatic action. For a PET measurement time of less than 1 h post injection, dephosphorylation (k_4) of the FDG-6-PO4 is not observed (Lucignani et al. 1993) and the assumption that $k_4 = 0$ is valid.

For radioligands with irreversible kinetic behavior, late static scanning can be considered (as is common for [^{18}F]-FDG PET) while these radioligands often provide high specific to nonspecific tracer concentration ratios. However, taking into account (2.28), a high affinity in terms of a large k_3^* means that influx rate constant K_i becomes proportional to K_1 and thus dependent on tracer transport rate from blood to the brain tissue. This way, K_i becomes less dependent of the parameter of interest k_3^* and therefore less sensitive to changes in binding site density. On the other hand, the slower equilibrium due to the slower irreversible kinetics of high affinity tracers imposes longer PET acquisition times to quantify potential changes in binding density as accurate as possible. However, quantification can be confounded by radio-metabolites entering the brain tissue. Many tracers currently used for imaging studies produce to some extent lipophilic metabolites. However, the quantities produced or their kinetics for passing the blood–brain barrier are such that they do not commonly confound the PET measurements. In cases where uptake and washout of the parent tracer are fast relative to the production and accumulation of radio-metabolites in plasma, their component of the total measured activity may be negligible during the imaging study. However, for longer PET acquisition times, lipophilic radio-metabolites may enter the brain in sufficient concentration to confound the PET signal.

In this context, preclinical micro-PET data of mice and rodents can provide useful information about tracer characteristics in terms of metabolization, kinetics, and nonspecific and (ir)reversible binding (Casteels et al. 2012) and prove to be a helpful tool in selecting the best possible tracer candidate for a specific target (Celen et al. 2010).

Although tracer characteristics can determine the compartmental model that best describes the in vivo process, biologically accurate models may not be practical. A model with higher complexity may be more accurate biologically but may have too many parameters, and hence it would be impossible to accurately estimate all of the model parameters. Some models might work when statistical noise is low but yield multiple solutions for high noise cases. Thus, model simplification may be required and some bias in parameter estimates will need to be allowed in order to obtain better precision. A number of configurations might have to be tested before choosing an appropriate model.

To illustrate reversible tracer kinetics, we present sample kinetic data of [^{11}C] verapamil (Fig. 2.4a), a PET tracer that allows the in vivo assessment of P-glycoprotein (P-gp) functionality in the blood–brain barrier (BBB). P-gp acts as an efflux pump playing a neuroprotective role by preventing many structurally divergent lipophilic molecules from entering the brain. However, it can also be a determinant factor in the treatment response to potential antipsychotic drugs. Suspected to be involved in several neurodegenerative and psychiatric brain disorders, P-gp function is reported to be regionally increased for patients with chronic schizophrenia (De Klerk et al. 2010) and major depressive disorder (De Klerk et al. 2009). Figure 2.4a compares a 1TCM and 2TCM describing the tracer kinetics of

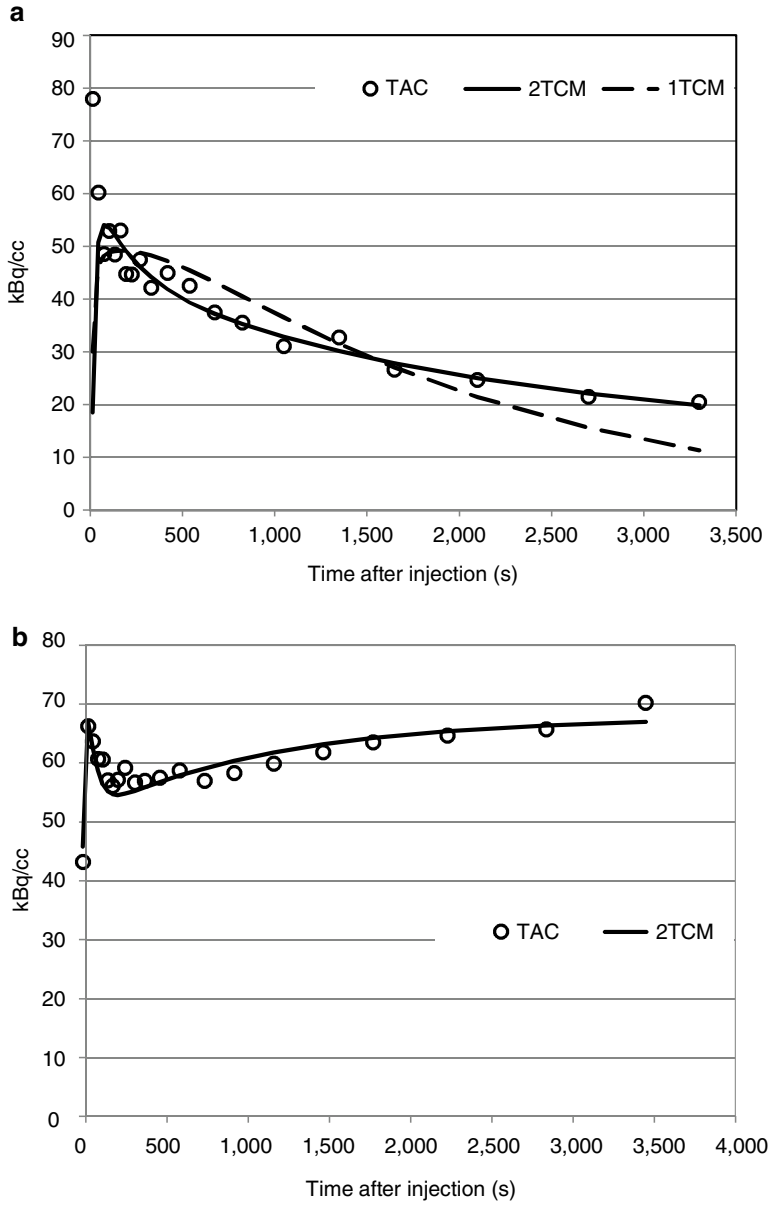

Fig. 2.4 (**a**) Comparison of fitting results of 1TCM and 2TCM fitted to the whole brain TAC of [^{11}C]verapamil using an arterial input function corrected for metabolites. (**b**) Representative TAC of [^{11}C]5-HTP uptake in a rodent brain, demonstrating irreversible tracer kinetics together with the fitting results of 2TCM with k_4 set to zero using an arterial input function corrected for metabolites

the whole brain uptake. The graph shows that 2TCM is clearly the more appropriate kinetic model for this particular PET tracer compared to 1TCM.

As an example of irreversible tracer kinetics, we evaluated the uptake of 5-hydroxy-L-[β-^{11}C]tryptophan ([^{11}C]5-HTP) in the rodent brain (Visser et al. 2013). [^{11}C]5-HTP will undergo the same conversions as 5-HTP which is the substrate for the enzymatic action of aromatic amino acid decarboxylase (AADC) for the production of 5-HT (Visser et al. 2011). Trapping rate of [^{11}C]5-HTP provides a quantitative measure for serotonin synthesis. Figure 2.4b presents the tracer kinetics of [^{11}C]5-HTP in the rodent brain, clearly demonstrating irreversible kinetics together with the fitting results of 2TCM with k_4 set to zero.

2.7 Graphical Analysis Methods

As described before, coupled linear differential equations formalize the exchange of substances between the compartments. Kinetic parameters can be estimated by fitting an analytical solution of these differential equations to the measured dynamic PET data. However, nonlinear fitting procedures are needed which are quite time-consuming and therefore of limited use to estimate the kinetic parameters on a voxel-by-voxel basis. However, the coupled differential equations can be reformulated in a linear form by transforming the arterial plasma data and measured dynamic PET data. Using this approach the transfer rate constant is in general not estimated separately, but information is restricted to the level of distribution volume V_T or metabolic rate K_i. On the other hand, a linear mathematical model, meaning that there is direct proportionality between model variables and measured data, allows optimal estimates to be computed directly in one iteration using linear regression. Consequently, these linear least-squares fitting methods are computationally very efficient and therefore very convenient for generating voxel-wise parametric image data. Moreover, graphical methods rely on the area under the curve of the measured data. Since, for a bolus injection, the peak contribution to the total area under the curve is limited while the tails of TACs are generally well estimated, these approaches are less sensitive to inaccuracies in peak estimation.

Demonstrating this approach for 1TCM, both sides of (2.4) can be integrated and written as

$$C_T(T) = K_1 \int_0^T C_P(t)\,dt - k_2 \int_0^T C_T(t)\,dt. \tag{2.29}$$

If we divide both sides by $C_T(T)$ and k_2 while taking into account that $V_T = \frac{K_1}{k_2}$, we get the following equation:

$$\frac{\int_0^T C_T(t)\,dt}{C_T(T)} = V_T \frac{\int_0^T C_T(t)\,dt}{C_T(T)} - \frac{1}{k_2}. \tag{2.30}$$

This form has originally been proposed by (Logan et al. 1990) where V_T can be identified with the slope of the resulting straight line. Actually, for this approach no explicit assumption is needed in terms of compartmental model. The only prerequisite is that the tracer demonstrates reversible binding such that V_T is a valid endpoint. For a true 1TCM, the Logan plot is linear at all times. In case of a 2TCM, the Logan plot becomes linear at later time points such that the slope of this linear part also provides an estimate for the tissue distribution volume V_T. A representative Logan plot is presented in Fig. 2.5a for the same kinetic data of [^{11}C]verapamil as shown in Fig. 2.4a. V_T estimates using the Logan plot are susceptible to

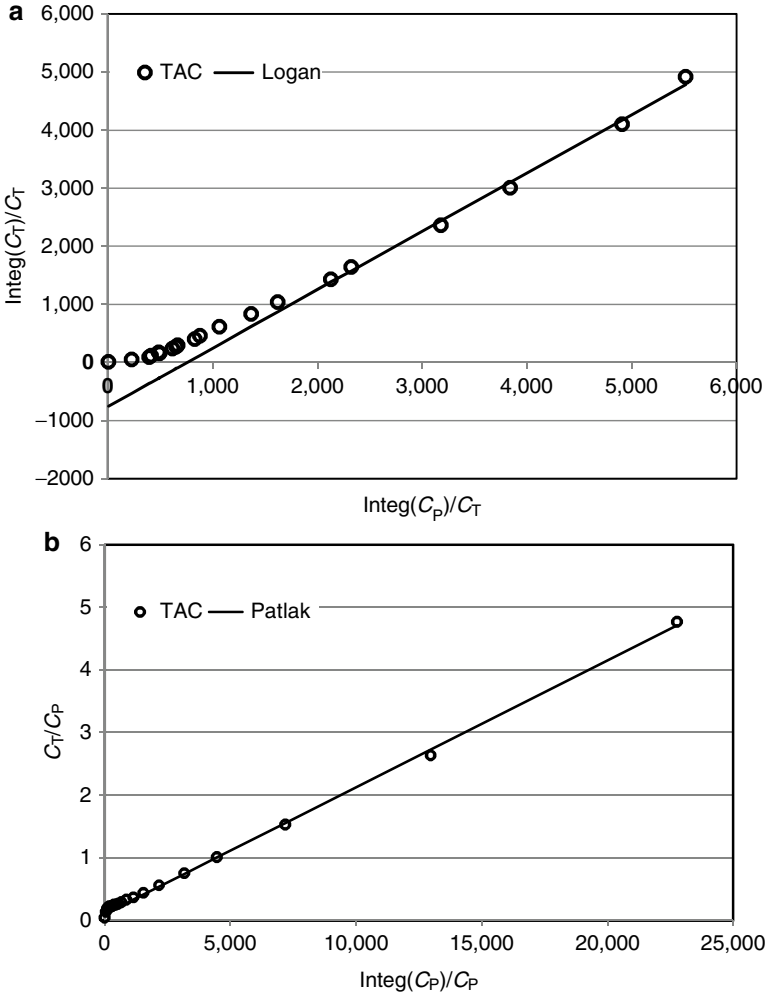

Fig. 2.5 (**a**) Logan plot for whole brain TAC of [^{11}C]verapamil using an arterial input function corrected for metabolites. (**b**) Patlak plot for whole brain TAC of [^{11}C]5-HTP in a rodent brain using an arterial input function corrected for metabolites

noise-induced bias. Several strategies have been proposed to decrease this bias at the expense of increased variability (Ichise et al. 2002; Logan et al. 2011).

While the Logan plot allows a linear regression analysis for a tracer demonstrating reversible binding, a graphical analysis approach can also be derived for a tracer with irreversible binding kinetics. Setting $k_4 = 0$ in (2.22) and (2.23), one gets the following equations:

$$\frac{\mathrm{d}C_{\mathrm{ND}}(t)}{\mathrm{d}t} = K_1 C_{\mathrm{P}}(t) - k_2 C_{\mathrm{ND}}(t) - k_3 C_{\mathrm{ND}}(t), \tag{2.31}$$

$$\frac{\mathrm{d}C_{\mathrm{S}}(t)}{\mathrm{d}t} = k_3 C_{\mathrm{ND}}(t). \tag{2.32}$$

If we assume that $C_{\mathrm{ND}}(t)$ and are in equilibrium, meaning that there is no net tracer transfer between the two compartments, the derivative in (2.31) can be set to zero and both sides of (2.32) can be integrated, yielding the following equation for the tracer concentration in tissue:

$$C_{\mathrm{T}}(T) = C_{\mathrm{ND}}(T) + C_{\mathrm{S}}(T) = V_{\mathrm{ND}}(T) C_{\mathrm{P}}(T) + \frac{K_1 k_3}{k_2 + k_3} \int_0^T C_{\mathrm{P}}(t)\,\mathrm{d}t. \tag{2.33}$$

If both sides of (2.33) are divided by the tracer concentration in plasma $C_{\mathrm{P}}(t)$, the following representation of the measured data is obtained:

$$\frac{C_{\mathrm{T}}(T)}{C_{\mathrm{P}}(T)} = V_{\mathrm{ND}}(T) + K_{\mathrm{i}} \frac{\int_0^T C_{\mathrm{P}}(t)\,\mathrm{d}t}{C_{\mathrm{P}}(T)}. \tag{2.34}$$

This linearization is called the Patlak plot. When tracer concentration of non-displaceable compartment and plasma are in equilibrium, the Patlak plot becomes linear and the metabolic rate K_{i} can be estimated as the slope of the linear part of the Patlak plot while the intercept provides an estimate for the distribution volume of the non-displaceable compartment. As an example, a Patlak analysis of the same dynamic PET data of [^{11}C]5-HTP, as presented in Fig. 2.4b, is shown in Fig. 2.5b.

Patlak analysis can be further simplified if the intersect is neglected and both sides of (2.34) are multiplied by $\frac{C_{\mathrm{P}}(T)}{\int_0^T C_{\mathrm{P}}(t')\,\mathrm{d}t}$ (Thie 1994). Thus, the metabolic rate can be approximated by

$$K_{\mathrm{i}} \approx \frac{C_{\mathrm{T}}(T)}{\int_0^T C_{\mathrm{P}}(t)\,\mathrm{d}t}. \tag{2.35}$$

If we assume that the PET signal is mainly determined by the tissue signal $C_{PET}(T) \cong C_T(T)$, K_i can be approximated by the fractional uptake ratio FUR defined as

$$\mathrm{FUR}(T) = \frac{C_{\mathrm{PET}}(T)}{\int_0^T C_P(t)\,\mathrm{d}t}. \tag{2.36}$$

FUR is also closely related to the standardized uptake value (SUV) defined as

$$\mathrm{SUV}(T) = \frac{C_{\mathrm{PET}}(T)}{\frac{\text{Injected Dose}}{\text{Weight}}}. \tag{2.37}$$

If we define $\frac{\text{Injected Dose}}{\text{Weight}}$ as a concentration C_{WB}, we can introduce a distribution volume V_{WB} defined as $V_{WB} = \frac{C_{WB}}{C_P(0)}$ and a plasma clearance rate k_p for time T defined as $k_P = \frac{C_P(0)}{\int_0^T C_P(t)\,\mathrm{d}t}$; the FUR is related to SUV by the relation

$$\mathrm{FUR}(T) = V_{WB} k_P(T) \mathrm{SUV}(T). \tag{2.38}$$

Therefore, FUR can be considered an approximation to the Patlak slope while FUR and SUV are proportional. Major disadvantage of SUV is that varying plasma dynamics are not taken into account. FUR and SUV have been successfully validated for the quantification of the specific binding of the CB1R tracer [^{18}F]MK-9470 in the human brain (Sanabria-Bohórquez et al. 2010).

2.8 Input Functions

For the quantification of the pharmacological parameters, dynamic PET data need to be accompanied by time-dependent activity concentrations of the intact tracer in arterial plasma. Arterial plasma tracer concentrations represent the delivery of the radiotracer to the system of interest and are mandatory as input function for the kinetic modeling of this system. In general, arterial blood sampling is performed during the PET acquisition where blood samples are collected through an arterial puncture, plasma is separated from the cellular blood fraction, and radioactivity in the plasma is corrected for any radiotracer molecules that might have undergone metabolism by enzymes in the plasma or the liver. This way a time-activity curve of the free intact radiotracer in plasma is obtained. This traditional approach however has a major drawback that drawing arterial blood samples is invasive for subjects and manual sampling requires substantial work for the PET personnel, although

automatic sampling can also be considered in a discrete or continuous fashion by means of blood samplers (Alf et al. 2013). Errors in arterial sampling may propagate into the quantification of system being studied. These errors can be due to incomplete or irregular sampling, sampling of small blood volumes yielding limited count statistics, and irregular or unreliable metabolite analysis. Moreover, additionally cross-calibration between the sample detection setup and the PET system needs to be secured.

Efforts have been made to determine the input function from the PET data by isolating the PET signal from the carotids. This noninvasive alternative to arterial sampling, denoted image-derived input function (IDIF), is however methodologically very challenging and has only been implemented successfully in clinical practice for a limited number of tracers (Zanotti-Fregonara et al. 2011a). Indeed, feasibility of IDIF depends on tracer kinetics after bolus injection and more specifically on an adequate carotid to background ratio which affects the accuracy of the image-derived whole blood activity concentration. On the other hand, even an acceptable IDIF will typically show inaccuracies in peak estimation. Impact of these peak errors on the quantitative parameters depends on the kinetic model and needs to be assessed for each tracer separately.

Other important limitations of IDIF are that the parent compound cannot be distinguished from its radioactive metabolites and that the plasma radioactivity cannot be separated from the whole blood activity concentration. In general, a limited numbers of blood samples is still needed to estimate differences between the plasma and whole blood activity concentration and to calculate the percentage of intact parent tracer in plasma (Sanabria-Bohórquez et al. 2000). To avoid arterial blood sampling, venous blood samples can be considered. However, arterial tracer kinetics can differ from the venous one, while only at late time points of the PET acquisition, the metabolite concentration reaches equilibrium between the arterial and venous compartment. Therefore, venous samples can be substituted for arterial samples but only for a limited time window that must be assessed individually for each tracer. In terms of metabolization, most neuro-receptor tracers have a high metabolite fraction and will therefore not be easily amenable to integrate an individualized metabolite correction with IDIF. One could consider an average metabolite curve while using late venous blood samples to estimate the radio-metabolite concentration and to scale the metabolite curve (Backes et al. 2009; Lammertsma et al. 1996). This type of metabolite correction is however not always possible and needs to be validated for every tracer.

Although with IDIF the number of arterial blood samples could at least be reduced, IDIF could only be used to its full extent for a limited number of PET tracers (Mourik et al. 2009; Zanotti-Fregonara et al. 2009, 2011b, c) and only rarely results in imaging procedures with reduced invasiveness for the patient. However, an IDIF approach allows to some extent to reduce the dependence of the quantification on reference devices such as well counter and dose calibrator. Therefore, this approach could prove more robust for possible incorrect cross-calibration with the PET system or be more sensitive to detect possible erroneous scaling.

A promising development to the IDIF approach is to parameterize the IDIF and to estimate these parameters simultaneously with the kinetic parameters describing tracer kinetics of several brain regions (Sanabria-Bohórquez 2003; Sanabria-Bohórquez et al. 2012). However, in practice some blood samples could be needed to improve the parameter estimation.

An alternative approach to IDIF is the use of a population-based input function created by normalizing individual input functions from a population of subjects and appropriately scaling this standard input function using venous or arterial blood samples. This approach has been validated primarily for [^{18}F]-FDG brain PET (Brock et al. 2005; Takagi et al. 2004), although this approach has been used for other tracers (Zanotti-Fregonara et al. 2012). However, one needs to keep in mind that an average input function obtained for a population of healthy subjects may not apply for a patient population because the disease state or treatment may affect tracer metabolization (Visvikis et al. 2004).

We have already described that BP_{ND} can be obtained from the DVR of the target region with specific tracer binding relative to the reference region devoid of specific binding if similar non-displaceable tracer concentration is assumed for both target and reference region. However, BP_{ND} can also be estimated from a reference tissue model where the TAC of the reference region is used as indirect input function to the kinetic model of the target region (Hume et al. 1992). This way neither blood samples nor labor-intensive radio-metabolite analysis is needed such that dependency on reference devices such as well counter or dose calibrator is completely avoided.

Instead of elaborating on a full reference tissue model which is based on 2TCM to describe tracer kinetics of a target region (Lammertsma et al. 1996), we will discuss the simplified reference tissue model (SRTM) (Lammertsma and Hume 1996) assuming tracer kinetics in both the target and reference region to be described adequately by a 1TCM. If we consider a 1TCM for target and reference region, we get the following equations (see (2.4)):

$$\frac{\mathrm{d}C_{\mathrm{T}}(t)}{\mathrm{d}t} = K_1 C_{\mathrm{P}}(t) - k_{2\mathrm{a}} C_{\mathrm{T}}(t), \tag{2.39}$$

$$\frac{\mathrm{d}C_{\mathrm{R}}(t)}{\mathrm{d}t} = K_{1\mathrm{R}} C_{\mathrm{P}}(t) - k_{2\mathrm{R}} C_{\mathrm{R}}(t). \tag{2.40}$$

$C_P(t)$ represents the plasma concentration of radioligand at time t, while $C_T(t)$ and $C_R(t)$ are instantaneous quantities denoting radioactivity concentration in the target and reference region, respectively. The subscript R refers to kinetics parameters of the reference region, while the subscript a refers to an "apparent" kinetic parameter. By assuming that the distribution volume of the nonspecifically bound tracer is the same in the reference and target region, the following equations can be derived by taking into account (2.9), (2.24), and (2.25):

$$V_{\mathrm{ND}} = \frac{K_1}{k_2} = \frac{K_{1\mathrm{R}}}{k_{2\mathrm{R}}}, \tag{2.41}$$

$$V_{\mathrm{T}} = \frac{K_1}{k_2}\left(1 + \mathrm{BP}_{\mathrm{ND}}\right) = \frac{K_1}{k_{2\mathrm{a}}}, \tag{2.42}$$

$$k_{2\mathrm{a}} = \frac{k_2}{1 + \mathrm{BP}_{\mathrm{ND}}}. \tag{2.43}$$

Solving (2.40) for $C_{\mathrm{P}}(t)$ gives the following expression for the tracer concentration in plasma:

$$C_{\mathrm{P}}\left(t\right) = \frac{1}{K_{1\mathrm{R}}}\left(\frac{\mathrm{d}C_{\mathrm{R}}\left(t\right)}{\mathrm{d}t} + k_{2\mathrm{R}}C_{\mathrm{R}}\left(t\right)\right). \tag{2.44}$$

Substitution of (2.44) in (2.39) and integrating both sides yields the following equation:

$$C_{\mathrm{T}}\left(T\right) = \frac{K_1}{K_{1\mathrm{R}}}C_{\mathrm{R}}\left(T\right) + \frac{K_1}{K_{1\mathrm{R}}}k_{2\mathrm{R}}\int_0^T C_{\mathrm{R}}\left(t\right)\mathrm{d}t - k_{2\mathrm{a}}\int_0^T C_{\mathrm{T}}\left(t\right)\mathrm{d}t. \tag{2.45}$$

If we define $R = \frac{K_1}{K_{1\mathrm{R}}} = \frac{k_2}{k_{2\mathrm{R}}}$, we get the following linear reference tissue model:

$$C_{\mathrm{T}}\left(T\right) = RC_{\mathrm{R}}\left(T\right) + k_2\int_0^T C_{\mathrm{R}}\left(t\right)\mathrm{d}t - k_{2\mathrm{a}}\int_0^T C_{\mathrm{T}}\left(t\right)\mathrm{d}t. \tag{2.46}$$

Expression (2.46) is similar as the multilinear reference tissue model (MRTM) (Ichise et al. 2003) and computationally efficient for voxel-wise estimation of $\mathrm{BP}_{\mathrm{ND}}$ image data. On the other hand, $\mathrm{BP}_{\mathrm{ND}}$ is the only achievable quantitative endpoint. Therefore, model validation using full kinetic modeling is essential, especially if non-displaceable tracer uptake could be affected by brain-penetrating radio-metabolites or disease-related permeability changes of the blood–brain barrier. Selection of the appropriate reference tissue should be supported by histology data and in vivo pre-clinical imaging. PET imaging after pre-dosing with a blocking agent which selectively binds to the same target with high affinity and is nontoxic at higher doses can confirm the choice for a specific brain region as reference tissue and can verify whether non-displaceable tracer uptake is similar for reference and target regions.

If, during a certain time interval of the dynamic PET data, the tracer concentration in brain tissue is in equilibrium with the tracer concentration in plasma, the reference tissue model can be further simplified and the DVR of target tissue relative to reference tissue as index for specific binding can be approximated by the SUV ratio of the target region relative to the reference region:

$$\mathrm{DVR} = \frac{V_T}{V_R} \cong \frac{C_T(T)}{C_R(T)} \cong \frac{C_{T,PET}(T)}{C_{R,PET}(T)} = \frac{\mathrm{SUV}_T(T)}{\mathrm{SUV}_R(T)} = \mathrm{SUVR}(T). \tag{2.47}$$

As an example, SUV ratios relative to the cerebellum have been used to quantify the brain retention of the Pittsburgh compound B (PIB), a PET tracer binding to amyloid deposits (Lopresti et al. 2005). However, this approximation needs validation with full kinetic modeling for each tracer separately.

2.9 Steady-State PET Measurements Using a Bolus/Constant Infusion

The tissue distribution volume V_T is defined as the ratio at equilibrium between tissue and plasma tracer concentration. Although equilibrium is not reached after fast bolus injection of a tracer, V_T can be estimated using dynamic PET scanning, plasma input function, and compartmental modeling (see (2.9), (2.19), and (2.24)). If a region without specific binding is available, the binding potential BP_{ND} can be estimated from the V_T values of the target and reference region (see (2.26)). Following a tracer bolus injection, tissue to plasma ratios and tissue ratios between different regions eventually become constant over time in case of reversible tracer binding. The tissue to plasma ratio of this transient equilibrium is called the apparent distribution volume V_{APP}. V_{APP} is biased compared to the true tissue distribution volume V_T because at transient equilibrium, tracer concentrations in blood and tissue are changing due to plasma clearance of tracer activity although ratios remain constant. In order to achieve constant tracer concentrations in tissue and blood, a constant infusion of the radiotracer can be given. Once steady-state conditions are reached, V_T can easily be determined as the ratio between the tissue concentration measured with a single PET scan $C_{T,PET}$ and the plasma activity of the intact tracer estimated using a single blood sample C_P:

$$V_T = \frac{C_{T,PET}}{C_P}. \tag{2.48}$$

In practice, multiple short PET scans and blood samples are acquired to demonstrate constant radioactivity levels in specific brain regions and in blood. If a brain region with no specific binding is available, no blood measurements are necessary and binding potential BP_{ND} can be calculated relative to the reference region as follows:

$$BP_{ND} = \frac{C_{T,PET} - C_{R,PET}}{C_{R,PET}}, \tag{2.49}$$

with $C_{R,PET}$ representing the PET tracer concentration measured in the reference region.

Major advantage of a bolus/infusion approach is the simple and straightforward quantification represented by (2.48) and (2.49) for which no model assumption is

required in terms of compartmental modeling. Using a single tracer synthesis, a bolus/infusion design provides powerful within-scan methodology for detecting changes in binding levels between control and stimulus conditions and measuring both exogenously and endogenously induced displacement of tracer binding (Carson et al. 1997). Additional advantage of a bolus/infusion approach is the reduced study time compared to two sequential bolus injection protocols. Furthermore, concentration differences between the arterial and venous blood compartment are likely to be small at equilibrium. This means that if blood activity measurements are needed for quantification, venous sampling might be adequate instead of the more invasive arterial sampling. Possible drawback is that only V_T can be estimated when measuring at equilibrium. Compartmental modeling of dynamic bolus studies on the other hand allows the estimation of individual rate parameters, such as K_1, as a measure of blood flow. One has to keep in mind however that the estimates for these individual rate constants can be biased by errors in the input function or by wrong assumptions about the selected model for the compartmental analysis. V_T on the other hand is generally accepted as a robust quantitative endpoint for PET neuro-receptor studies.

A priming bolus injection can precede the constant tracer infusion to accelerate the process of establishing true equilibrium. This acceleration of reaching steady state is important because of the short half-life of PET tracers. In practice, a bolus/infusion approach is better suited for PET studies with [^{18}F]-labeled tracers or tracers with even a longer half-life, while the statistical quality of bolus injection studies is expected to be better for short-lived PET tracers. However, optimization of the bolus/infusion protocol in terms of timing and noise reduction should increase the sensitivity for the detection of biological signals (Watabe et al. 2000).

Of particular interest is the optimal ratio between priming bolus and infusion dose which is region dependent since regions with high specific binding and therefore slower kinetics require longer time to reach equilibrium (Pinborg et al. 2000). Based on data from previous bolus injection experiments, the optimal dose balance between priming bolus and infusion can be estimated. However, this optimal balance can be subject to individual and group differences due to changes in peripheral tracer metabolism.

References

Alf MF, Wyss MT, Buck A et al (2013) Quantification of brain glucose metabolism by 18F-FDG PET with real-time arterial and image-derived input function in mice. J Nucl Med 54:132–138. doi:10.2967/jnumed.112.107474

Backes H, Ullrich R, Neumaier B et al (2009) Noninvasive quantification of 18F-FLT human brain PET for the assessment of tumour proliferation in patients with high-grade glioma. Eur J Nucl Med Mol Imaging 36:1960–1967. doi:10.1007/s00259-009-1244-4

Bender AT, Beavo JA (2006) Cyclic nucleotide phosphodiesterases: molecular regulation to clinical use. Pharmacol Rev 58:488–520. doi:10.1124/pr.58.3.5.488

Brock CS, Young H, Osman S et al (2005) Glucose metabolism in brain tumours can be estimated using [18F]2-fluorodeoxyglucose positron emission tomography and a population-derived input function scaled using a single arterialised venous blood sample. Int J Oncology 26:1377–1383

Carson RE, Breier A, De Bartolomeis A et al (1997) Quantification of amphetamine-induced changes in [11C]raclopride binding with continuous infusion. J Cereb Blood Flow Metab 17:437–447. doi:10.1097/00004647-199704000-00009

Casteels C, Koole M, Celen S et al (2012) Preclinical evaluation and quantification of [^{18}F] MK-9470 as a radioligand for PET imaging of the type 1 cannabinoid receptor in rat brain. Eur J Nucl Med Mol Imaging 39:1467–1477. doi:10.1007/s00259-012-2163-3

Celen S, Koole M, De Angelis M et al (2010) Preclinical evaluation of 18F-JNJ41510417 as a radioligand for PET imaging of phosphodiesterase-10A in the brain. J Nucl Med 51:1584–1591. doi:10.2967/jnumed.110.077040

Crone C (1963) The permeability of capillaries in various organs as determined by use of the "indicator diffusion" method. Acta Physiol Scand 58:292–305

De Klerk OL, Willemsen ATM, Roosink M et al (2009) Locally increased P-glycoprotein function in major depression: a PET study with [11C]verapamil as a probe for P-glycoprotein function in the blood–brain barrier. Int J Neuropsychopharmacol 12:895–904. doi:10.1017/S1461145709009894

De Klerk OL, Willemsen ATM, Bosker FJ et al (2010) Regional increase in P-glycoprotein function in the blood–brain barrier of patients with chronic schizophrenia: a PET study with [(11)C]verapamil as a probe for P-glycoprotein function. Psychiatry Res 183:151–156. doi:10.1016/j.pscychresns.2010.05.002

Doorduin J, De Vries EFJ, Willemsen ATM et al (2009) Neuroinflammation in schizophrenia-related psychosis: a PET study. J Nucl Med 50:1801–1807. doi:10.2967/jnumed.109.066647

Duman RS, Aghajanian GK (2012) Synaptic dysfunction in depression: potential therapeutic targets. Science (New York, NY) 338:68–72. doi:10.1126/science.1222939

Enzi B, Duncan NW, Kaufmann J et al (2012) Glutamate modulates resting state activity in the perigenual anterior cingulate cortex – a combined fMRI-MRS study. Neuroscience 227:102–109. doi:10.1016/j.neuroscience.2012.09.039

Frackowiak RS, Lenzi GL, Jones T, Heather JD (1980) Quantitative measurement of regional cerebral blood flow and oxygen metabolism in man using 15O and positron emission tomography: theory, procedure, and normal values. J Comput Assist Tomogr 4:727–736

Fujishige K, Kotera J, Omori K (1999) Striatum- and testis-specific phosphodiesterase PDE10A isolation and characterization of a rat PDE10A. Eur J Biochem 266:1118–1127

Gérard N, Pieters G, Goffin K et al (2011) Brain type 1 cannabinoid receptor availability in patients with anorexia and bulimia nervosa. Biol Psychiatry 70:777–784. doi:10.1016/j.biopsych.2011.05.010

Grauer SM, Pulito VL, Navarra RL et al (2009) Phosphodiesterase 10A inhibitor activity in preclinical models of the positive, Cognitive, and Negative Symptoms of schizophrenia. J Pharmacol Exp Ther 331:574–590. doi:10.1124/jpet.109.155994

Greicius M (2008) Resting-state functional connectivity in neuropsychiatric disorders. Curr Opin Neurol 21:424–430. doi:10.1097/WCO.0b013e328306f2c5

Hebb ALO, Robertson HA (2007) Role of phosphodiesterases in neurological and psychiatric disease. Curr Opin Pharmacol 7:86–92. doi:10.1016/j.coph.2006.08.014

Hebb A, Robertson H, Denovan-Wright E (2004) Striatal phosphodiesterase mRNA and protein levels are reduced in Huntington's disease transgenic mice prior to the onset of motor symptoms. Neuroscience 123:967–981. doi:10.1016/j.neuroscience.2003.11.009

Hirvonen J, Zanotti-Fregonara P, Umhau JC et al (2012) Reduced cannabinoid CB(1) receptor binding in alcohol dependence measured with positron emission tomography. Mol Psychiatry. doi:10.1038/mp.2012.100

Hume SP, Myers R, Bloomfield PM et al (1992) Quantitation of carbon-11-labeled raclopride in rat striatum using positron emission tomography. Synapse (New York, NY) 12:47–54. doi:10.1002/syn.890120106

Ichise M, Toyama H, Innis RB, Carson RE (2002) Strategies to improve neuroreceptor parameter estimation by linear regression analysis. J Cereb Blood Flow Metab 22:1271–1281. doi:10.1097/00004647-200210000-00015

Ichise M, Liow J-S, Lu J-Q et al (2003) Linearized reference tissue parametric imaging methods: application to [11C]DASB positron emission tomography studies of the serotonin transporter

in human brain. J Cereb Blood Flow Metab 23:1096–1112. doi:10.1097/01.WCB.0000085441.37552.CA

Innis RB, Carson R (2007) Consensus nomenclature: its time has come. Eur J Nucl Med Mol Imaging 34:1239. doi:10.1007/s00259-007-0481-7

Kendell SF, Krystal JH, Sanacora G (2005) GABA and glutamate systems as therapeutic targets in depression and mood disorders. Expert Opin Ther Targets 9:153–168. doi:10.1517/14728222.9.1.153

Kenneth LD, Dennis C, Joseph TC, Nemeroff C (2002) Neuropsychopharmacology—the fifth generation of progress, first edit. 2080. In: Davis KL, Charney D, Coyle JT, Nemeroff Lippincott C (eds), Williams and Wilkins: Philadelphia, 2002. ISBN: 0-7817-2837-1

Kety SS, Schmidt CF (1948) The nitrous oxide method for the quantitative determination of cerebral blood flow in man: theory, procedure and normal values. J Clin Invest 27:476–483. doi:10.1172/JCI101994

Kim J-J, Park H-J, Jung Y-C et al (2009) Evaluative processing of ambivalent stimuli in patients with schizophrenia and depression: a [15O] H2O PET study. J Int Neuropsychol Soc 15:990–1001. doi:10.1017/S1355617709990403

Kühn S, Gallinat J (2013) Resting-state brain activity in schizophrenia and major depression: a quantitative meta-analysis. Schizophr Bull 39:358–365. doi:10.1093/schbul/sbr151

Lammertsma AA, Hume SP (1996) Simplified reference tissue model for PET receptor studies. Neuroimage 4:153–158. doi:10.1006/nimg.1996.0066

Lammertsma AA, Bench CJ, Hume SP et al (1996) Comparison of methods for analysis of clinical [11C]raclopride studies. J Cereb Blood Flow Metab 16:42–52. doi:10.1097/00004647-199601000-00005

Logan J, Fowler JS, Volkow ND et al (1990) Graphical analysis of reversible radioligand binding from time-activity measurements applied to [N-11C-methyl]-(−)-cocaine PET studies in human subjects. J Cereb Blood Flow Metab 10:740–747. doi:10.1038/jcbfm.1990.127

Logan J, Alexoff D, Fowler JS (2011) The use of alternative forms of graphical analysis to balance bias and precision in PET images. J Cereb Blood Flow Metab 31:535–546. doi:10.1038/jcbfm.2010.123

Lopresti BJ, Klunk WE, Mathis CA et al (2005) Simplified quantification of Pittsburgh Compound B amyloid imaging PET studies: a comparative analysis. J Nucl Med 46:1959–1972

Lucignani G, Schmidt KC, Moresco RM et al (1993) Measurement of regional cerebral glucose utilization with fluorine-18-FDG and PET in heterogeneous tissues: theoretical considerations and practical procedure. J Nucl Med 34:360–369

Luyten L, Casteels C, Vansteenwegen D et al (2012) Micro-positron emission tomography imaging of rat brain metabolism during expression of contextual conditioning. J Neurosci 32:254–263. doi:10.1523/JNEUROSCI.3701-11.2012

Menniti FS, Faraci WS, Schmidt CJ (2006) Phosphodiesterases in the CNS: targets for drug development. Nat Rev Drug Discov 5:660–670. doi:10.1038/nrd2058

Mourik JEM, Lubberink M, Schuitemaker A et al (2009) Image-derived input functions for PET brain studies. Eur J Nucl Med Mol Imaging 36:463–471. doi:10.1007/s00259-008-0986-8

Nishi A, Kuroiwa M, Miller DB et al (2008) Distinct roles of PDE4 and PDE10A in the regulation of cAMP/PKA signaling in the striatum. J Neurosci 28:10460–10471. doi:10.1523/JNEUROSCI.2518-08.2008

Phelps ME, Huang SC, Hoffman EJ et al (1979) Tomographic measurement of local cerebral glucose metabolic rate in humans with (F-18)2-fluoro-2-deoxy-D-glucose: validation of method. Ann Neurol 6:371–388. doi:10.1002/ana.410060502

Pinborg LH, Videbaek C, Knudsen GM et al (2000) Dopamine D(2) receptor quantification in extrastriatal brain regions using [(123)I]epidepride with bolus/infusion. Synapse (New York, NY)36:322–329,doi:10.1002/(SICI)1098-2396(20000615)36:4<322::AID-SYN9>3.0.CO;2-W

Puts NAJ, Edden RAE (2012) In vivo magnetic resonance spectroscopy of GABA: a methodological review. Prog Nucl Magn Reson Spectrosc 60:29–41. doi:10.1016/j.pnmrs.2011.06.001

Renkin EM (1959) Exchangeability of tissue potassium in skeletal muscle. Am J Physiol 197:1211–1215

Rousset O, Rahmim A, Alavi A, Zaidi H (2007) Partial volume correction strategies in PET. PET Clin 2:235–249. doi:10.1016/j.cpet.2007.10.005

Sanabria-Bohórquez S (2003) Image-derived input function for [11C]flumazenil kinetic analysis in human brain. Mol Imaging Biol 5:72–78. doi:10.1016/S1536-1632(03)00046-5

Sanabria-Bohórquez SM, Labar D, Levêque P et al (2000) [11C]flumazenil metabolite measurement in plasma is not necessary for accurate brain benzodiazepine receptor quantification. Eur J Nucl Med 27:1674–1683

Sanabria-Bohórquez SM, Hamill TG, Goffin K et al (2010) Kinetic analysis of the cannabinoid-1 receptor PET tracer [(18)F]MK-9470 in human brain. Eur J Nucl Med Mol Imaging 37:920–933. doi:10.1007/s00259-009-1340-5

Sanabria-Bohórquez SM, Joshi AD, Holahan M et al (2012) Quantification of the glycine transporter 1 in rhesus monkey brain using [18F]MK-6577 and a model-based input function. Neuroimage 59:2589–2599. doi:10.1016/j.neuroimage.2011.08.080

Sanacora G, Treccani G, Popoli M (2012) Towards a glutamate hypothesis of depression: an emerging frontier of neuropsychopharmacology for mood disorders. Neuropharmacology 62:63–77. doi:10.1016/j.neuropharm.2011.07.036

Savitz JB, Drevets WC (2013) Neuroreceptor imaging in depression. Neurobiol Dis 52:49–65. doi:10.1016/j.nbd.2012.06.001

Seeger TF, Bartlett B, Coskran TM et al (2003) Immunohistochemical localization of PDE10A in the rat brain. Brain Res 985:113–126

Siuciak JA, Strick CA (2006) Treating neuropsychiatric disorders with PDE10A inhibitors. Drug Discov Today Ther Strateg 3:527–532. doi:10.1016/j.ddstr.2006.10.012

Smith DF, Jakobsen S (2009) Molecular tools for assessing human depression by positron emission tomography. Eur Neuropsychopharmacol 19:611–628. doi:10.1016/j.euroneuro.2009.04.005

Surmeier DJ, Ding J, Day M et al (2007) D1 and D2 dopamine-receptor modulation of striatal glutamatergic signaling in striatal medium spiny neurons. Trends Neurosci 30:228–235. doi:10.1016/j.tins.2007.03.008

Svarer C, Madsen K, Hasselbalch SG et al (2005) MR-based automatic delineation of volumes of interest in human brain PET images using probability maps. Neuroimage 24:969–979. doi:10.1016/j.neuroimage.2004.10.017

Takagi S, Takahashi W, Shinohara Y et al (2004) Quantitative PET cerebral glucose metabolism estimates using a single non-arterialized venous-blood sample. Ann Nucl Med 18:297–302

Thie JA (1994) Clarification of a fractional uptake concept. Comment on Effects of hyperglycemia on FDG uptake in human brain and glioma. J Nucl Med. 36(4):711–712

Tu Z, Fan J, Li S et al (2011) Radiosynthesis and in vivo evaluation of [11C]MP-10 as a PET probe for imaging PDE10A in rodent and non-human primate brain. Bioorg Med Chem 19:1666–1673. doi:10.1016/j.bmc.2011.01.032

Van Laere K, De Hoon J, Bormans G et al (2012) Equivalent dynamic human brain NK1-receptor occupancy following single-dose i.v. fosaprepitant vs. oral aprepitant as assessed by PET imaging. Clin Pharmacol Ther 92:243–250. doi:10.1038/clpt.2012.62

Van Laere K, Ahmad RU, Hudyana H et al (2013) Human biodistribution and dosimetry of 18F-JNJ42259152, a radioligand for phosphodiesterase 10A imaging. Eur J Nucl Med Mol Imaging 40:254–261. doi:10.1007/s00259-012-2270-1

Visser AK, Ramakrishnan NK, Willemsen AT et al (2013). [11C]5-HTP and microPET are not suitable for pharmacodynamic studies in the rodent brain. J Cereb Blood Flow Metab. doi:10.1038/jcbfm.2013.171. [Epub ahead of print]

Visser AKD, Van Waarde A, Willemsen ATM et al (2011) Measuring serotonin synthesis: from conventional methods to PET tracers and their (pre)clinical implications. Eur J Nucl Med Mol Imaging 38:576–591. doi:10.1007/s00259-010-1663-2

Visvikis D, Francis D, Mulligan R et al (2004) Comparison of methodologies for the in vivo assessment of 18FLT utilisation in colorectal cancer. Eur J Nucl Med Mol Imaging 31:169–178. doi:10.1007/s00259-003-1339-2

Walter M, Henning A, Grimm S et al (2009) The relationship between aberrant neuronal activation in the pregenual anterior cingulate, altered glutamatergic metabolism, and anhedonia in major depression. Arch Gen Psychiatry 66:478–486. doi:10.1001/archgenpsychiatry.2009.39

Watabe H, Endres CJ, Breier A et al (2000) Measurement of dopamine release with continuous infusion of [11C]raclopride: optimization and signal-to-noise considerations. J Nucl Med 41:522–530

Wong DF, Kuwabara H, Horti AG et al (2010) Quantification of cerebral cannabinoid receptors subtype 1 (CB1) in healthy subjects and schizophrenia by the novel PET radioligand [11C] OMAR. Neuroimage 52:1505–1513. doi:10.1016/j.neuroimage.2010.04.034

Zanotti-Fregonara P, Fadaili EM, Maroy R et al (2009) Comparison of eight methods for the estimation of the image-derived input function in dynamic [(18)F]-FDG PET human brain studies. J Cereb Blood Flow Metab 29:1825–1835. doi:10.1038/jcbfm.2009.93

Zanotti-Fregonara P, Chen K, Liow J-S et al (2011a) Image-derived input function for brain PET studies: many challenges and few opportunities. J Cereb Blood Flow Metab 31:1986–1998. doi:10.1038/jcbfm.2011.107

Zanotti-Fregonara P, Liow J-S, Fujita M et al (2011b) Image-derived input function for human brain using high resolution PET imaging with [C](R)-rolipram and [C]PBR28. PLoS One 6:e17056. doi:10.1371/journal.pone.0017056

Zanotti-Fregonara P, Zoghbi SS, Liow J-S et al (2011c) Kinetic analysis in human brain of [11C](R)-rolipram, a positron emission tomographic radioligand to image phosphodiesterase 4: a retest study and use of an image-derived input function. Neuroimage 54:1903–1909. doi:10.1016/j.neuroimage.2010.10.064

Zanotti-Fregonara P, Hines CS, Zoghbi SS et al (2012) Population-based input function and image-derived input function for [^{11}C](R)-rolipram PET imaging: methodology, validation and application to the study of major depressive disorder. Neuroimage 63:1532–1541. doi:10.1016/j.neuroimage.2012.08.007